NANO LETTERS

Letter

pubs.acs.org/NanoLett

Template-Free Preparation of Crystalline Ge Nanowire Film Electrodes via an Electrochemical Liquid–Liquid–Solid Process in Water at Ambient Pressure and Temperature for Energy Storage

Junsi Gu,[†] Sean M. Collins,[†] Azhar I. Carim,[†] Xiaoguang Hao,[†] Bart M. Bartlett,[†] and Stephen Maldonado[†,‡,*]

[†]Chemistry Department, University of Michigan, 930 North University, Ann Arbor, Michigan 48109, United States

[‡]Applied Physics Program, University of Michigan, 450 Church Street, Ann Arbor, Michigan 48109, United States

Supporting Information

ABSTRACT: The direct electrodeposition of crystalline germanium (Ge) nanowire film electrodes from an aqueous solution of dissolved GeO_2 using discrete 'flux' nanoparticles capable of dissolving Ge(s) has been demonstrated. Electrodeposition of Ge at inert electrode substrates decorated with small (<100 nm), discrete indium (In) nanoparticles resulted in crystalline Ge nanowire films with definable nanowire diameters and densities without the need for a physical or chemical template. The Ge nanowires exhibited strong polycrystalline character as-deposited, with approximate crystallite dimensions of 20 nm and a mixed orientation of the crystallites along the length of the nanowire. Energy dispersive spectroscopic elemental mapping of individual Ge nanowires showed that the In nanoparticles remained at the base of each nanowire, indicating good electrical communication between the Ge nanowire and the underlying conductive support. As-deposited Ge nanowire films prepared on Cu supports were used without further processing as Li^+ battery anodes. Cycling studies performed at 1 C (1624 mA g^{-1}) indicated the native Ge nanowire films supported stable discharge capacities at the level of 973 mA h g^{-1}, higher than analogous Ge nanowire film electrodes prepared through an energy-intensive vapor–liquid–solid nanowire growth process. The cumulative data show that ec-LLS is a viable method for directly preparing a functional, high-activity nanomaterials-based device component. The work presented here is a step toward the realization of simple processes that make fully functional energy conversion/storage technologies based on crystalline inorganic semiconductors entirely through benchtop, aqueous chemistry and electrochemistry without time- or energy-intensive process steps.

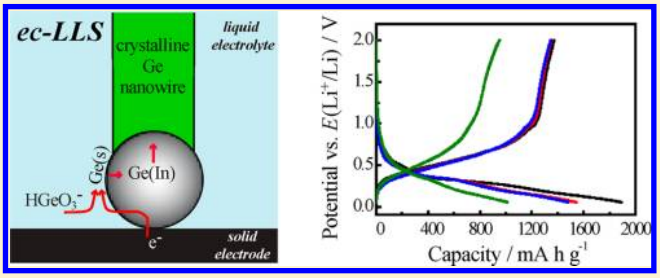

KEYWORDS: *Germanium nanowires, ec-LLS, electrodeposition, lithium-ion battery anodes*

Scalable, nonenergy intensive, and environmentally benign methods for producing crystalline, nanostructured semiconductor materials are paramount to advance next generation energy conversion/storage technologies.[1,2] To this end, assembly strategies that do not rely on existing semiconductor industry fabrication practices[2] but instead yield fully functional nanomaterials-based devices in a single preparative step need to be demonstrated.[3] Our group recently discovered a new route for electrochemically synthesizing crystalline semiconductor nanowires under benchtop conditions in aqueous electrolytes.[4] Our strategy utilizes a metallic liquid 'flux' electrode that acts both as a traditional electrode platform for electrodeposition as well as a solvent for crystallization.[4] In this approach, the semiconductor is initially electrodeposited as a fully reduced material and then is dissolved within the 'flux' electrode. If the electrodeposition is allowed to continue, the alloy eventually reaches saturation, followed by crystalline semiconductor precipitation out of the 'flux' electrode. The crystallinity and morphology of the deposit are strongly governed by the rates of electroreduction, dissolution, crystal nucleation, and precipitation. In this way, our method combines elements of more familiar semiconductor nanowire preparative techniques, such as vapor–liquid–solid (VLS)[5] and solution–liquid–solid (SLS)[6] growths with traditional metal flux crystallizations,[7,8] under the auspice of complete electrochemical control. Accordingly, we have dubbed it an electrochemical liquid–liquid–solid (ec-LLS) semiconductor crystal growth.

Individual metal 'flux' nanoparticles dispersed on an inert solid electrode support are potentially more amenable than bulk liquid metal pools for exploiting the ec-LLS process to synthesize an electrical/electrochemical device component. Discrete, closely spaced liquid metal (e.g., Hg) droplets are somewhat problematic due to the tendency to coalesce.[9] Less mobile 'flux' materials like indium (In) nanoparticles are a possible alternative. Although bulk In has a moderately low-melting point (ca. 157 °C), a surface melting point near 100

Received: May 22, 2012
Revised: July 26, 2012

   dx.doi.org/10.1021/nl301912f | *Nano Lett.* XXXX, XXX, XXX–XXX

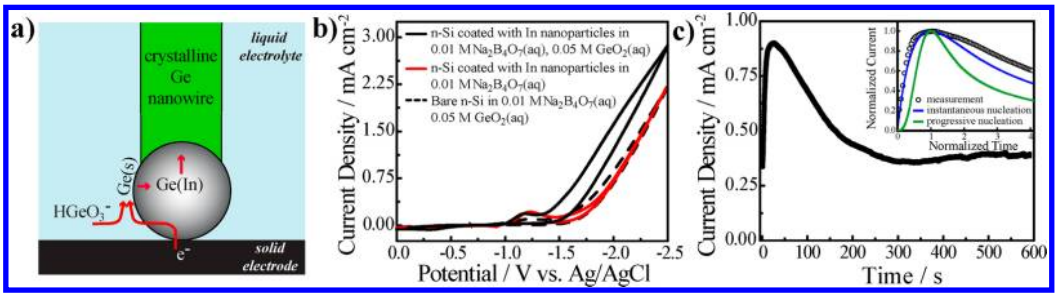

Figure 1. (a) Schematic depiction of ec-LLS process for Ge nanowire electrodeposition at an In nanoparticle 'flux' electrode on an inert conductive substrate. (b) Current−potential responses for n-Si electrodes immersed in 0.01 M $Na_2B_4O_7$ (aq). Responses are shown for (dashed line) bare n-Si electrodes in electrolyte with 0.05 M GeO_2 (aq), (solid red line) n-Si electrodes decorated with In nanoparticles in electrolyte without 0.05 M GeO_2 (aq), and (solid black line) n-Si electrodes decorated with In nanoparticles in electrolyte with 0.05 M GeO_2 (aq). Scan rate = 0.025 V s^{-1}. (c) Corrected current−time response for n-Si electrode coated with In nanoparticles, immersed in 0.01 M $Na_2B_4O_7$ (aq) and 0.05 M GeO_2 (aq) and biased at −2.0 V vs Ag/AgCl for 10 min. Inset: Same data with current normalized to the peak current density and time normalized to the time corresponding to the peak current density. Models for (blue line) instantaneous and (green line) progressive nucleation models are also shown.

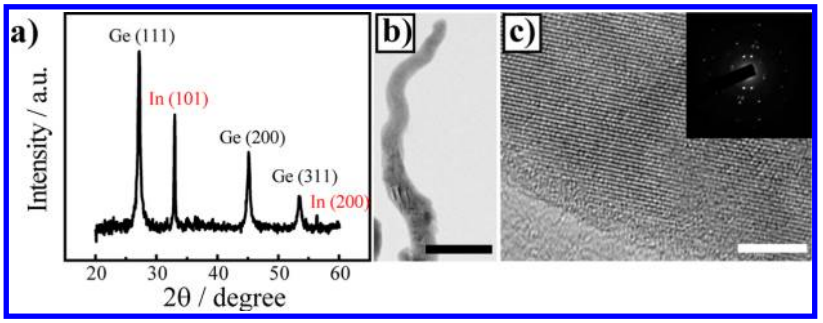

Figure 2. (a) Measured X-ray diffraction pattern collected after Ge electrodeposition at −2.0 V vs Ag/AgCl for 1 h. (b) Transmission electron micrograph of an individual Ge nanowire electrodeposited at −2.0 V vs Ag/AgCl for 10 min. Scale bar: 50 nm. (c) High-resolution transmission electron micrograph of same Ge nanowire as in (b). Scale bar: 5 nm. Inset: selected area electron diffraction pattern indicating a diamond cubic lattice.

°C,[10] and a melting point of small In nanoparticles below 100 °C,[11,12] In is not typically considered a liquid metal at room temperature. However, separate studies have shown that In nanoparticles specifically in intimate contact with Ge have an unusually low-melting point, with In−Ge nanoparticles apparently showing liquid properties at room temperature.[13] This large melting point depression has been rationalized to arise from large heteroepitaxial stress between two dissimilar materials.[13,14] We posit that In nanoparticles prepared on a conductive support that is otherwise inactive toward Ge electrodeposition may thus be a stable and ideal platform for ec-LLS preparation of individual Ge nanowire film electrodes (Figure 1a).

This letter addresses the hypothesis that ec-LLS can be used as a simple benchtop, potentially scalable, and non-energy intensive method for making energy technologies. The data shown here demonstrate three important discoveries: (1) ec-LLS can be performed on supported nanosized flux electrodes, (2) the ec-LLS process is not specific to Hg and can be performed with attractive flux materials, like In, and (3) crystalline Ge nanowire films with readily tunable properties can be used as active nanostructured device electrodes as-prepared. As a proof of concept for the utility of ec-LLS, as-electrodeposited Ge nanowire film electrodes are shown with high Li^+ charge/discharge capacities.

RESULTS AND DISCUSSION

Figure 1b summarizes the current−potential responses for n-Si electrodes coated with In nanoparticles for the electrodeposition of Ge nanowires via ec-LLS. Bare n-Si electrodes immersed in aqueous electrolyte with dissolved GeO_2 showed no evidence of Ge electrodeposition at any applied potential in this electrolyte, in accord with past reports of Ge electrodeposition.[15,16] These electrodes also yielded similar current−potential responses as n-Si electrodes coated with In nanoparticles immersed in aqueous electrolyte without dissolved GeO_2, indicating that the presence of In nanoparticles did not substantially enhance the observable activity for H_2 evolution at negative applied potentials, in agreement with the known poor electrocatalytic activity of In for H^+ reduction.[17] In an aqueous electrolyte containing dissolved GeO_2, n-Si electrodes coated with In nanoparticles showed uniformly higher current densities at potentials more negative than −1.4 V vs Ag/AgCl, in accord with the notion that the reduction of dissolved GeO_2 occurred exclusively at the In nanoparticles. Chronoamperometric experiments showed that the Ge electrodeposition process was unabated over the entire time (Figure S1, Supporting Information). These electrodes visibly darkened during the course of electrodeposition, eventually becoming dull black (vide infra). Figure 1c illustrates data from a current transient (corrected for contribution from faradaic current from H^+ reduction, Supporting Information) from a chronoamperometric experiment with an n-Si electrode coated with In nanoparticles immersed in an aqueous electrolyte with 0.05 M GeO_2 (aq) and biased at −2.0 V vs Ag/AgCl. These experiments consistently showed a peaked profile mirroring the shape typically observed in data for chronoamperometric electrodepositions.[18] The inset to Figure 1c shows the

dx.doi.org/10.1021/nl301912f | Nano Lett. XXXX, XXX, XXX−XXX

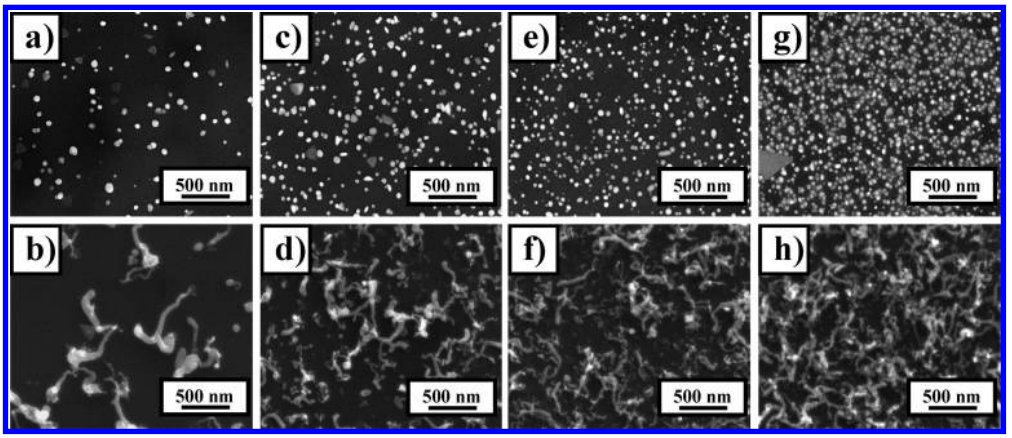

Figure 3. Top-down view scanning electron micrographs of n-Si electrodes decorated with different densities of In nanoparticles before and after (a and b; c and d; e and f; g and h) Ge electrodeposition at −2.0 V vs Ag/AgCl for 10 min.

normalized current−time response in relation to the expected transient response from the two prevailing models (instantaneous and progressive nucleation) for electrodeposition processes.[18,19] The collected data at short times agreed well with the instantaneous nucleation model, suggesting Ge electrodeposition occurred immediately at a finite number of In nanoparticles (i.e., the electrodeposition of each Ge nanowire in the film began instantly and uniformly rather than a progressive initiation of additional Ge nanowires throughout the potential step experiment).

Figure 2 describes the crystallinity of the as-prepared Ge nanowires. Following Ge electrodeposition at −2.0 V vs Ag/AgCl for 60 min, electrodes were removed from solution and dried under N_2 (g). Figure 2a shows the observed X-ray diffraction patterns for these as-prepared materials, indicating crystalline Ge with the expected diamond cubic lattice. Line broadening indicated a mean crystalline size of ∼20 nm, and the pattern of reflections corresponded to a lattice constant of 5.67 Å, in good agreement with the expected lattice constant of 5.66 Å for bulk crystalline Ge. Separate transmission electron microscopy performed on as-prepared Ge nanowires similarly showed evidence of strong crystalline character. Figure 2b,c indicates the Ge nanowires were not single crystalline but rather polycrystalline (as evidenced by variations in contrast and the polycrystalline pattern in selected area electron diffraction) with grain sizes in accord with those noted from X-ray diffraction. These features were broadly consistent with the Ge nanowires in our previous report,[4] although the crystallite sizes were larger here. Further, high magnification micrographs (Figure 2c and Figure S2, Supporting Information) showed that the polycrystalline grains were of mixed but not purely random orientation, i.e., the orientation of one crystallite was related to the orientation of adjacent crystallites. From the observed lattice fringes and the inset in Figure 2c, the distance between the (111) planes, d_{111}, was estimated as 3.29 Å, in reasonable accord with the known d_{111} value of 3.26 Å for diamond cubic Ge.

Figures 3 and 4 highlight the influence of the In nanoparticles on the resultant features of the Ge nanowires. As shown in the top-down scanning electron micrographs in Figure 3a,c,e,g, experiments were performed on n-Si electrodes with varied loadings of In nanoparticles controlled through the parameters used for In electrodeposition. The densities and sizes of In nanoparticles were controlled solely through the applied potential used to electrodeposit In from solution

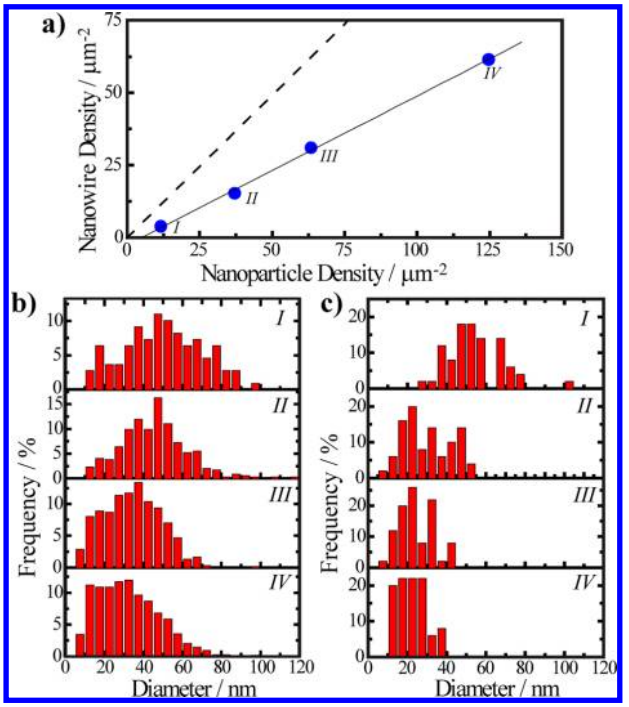

Figure 4. (a) Comparison of the observed density of Ge nanowires as a function of the observed density of In nanoparticles on n-Si electrodes. Dashed line corresponds to 1 Ge nanowire per 1 In nanoparticle. (b) Observed size distribution of In nanoparticles at several different In nanoparticle densities, as indicated in (a). (c) Size distribution of Ge nanowires electrodeposited from In nanoparticles at the four different densities of In nanoparticles shown in (b). Bin sizes in (b) and (c) are 5 nm.

(Supporting Information). Through this preparation, the average size of In nanoparticles tended to decrease as the density of In nanoparticles was increased. Each of these n-Si platforms loaded with In nanoparticles was then subject to the same Ge electrodeposition step at −2.0 V vs Ag/AgCl lasting 10 min. Three points are visually apparent from the micrographs in Figure 3: First, the density of Ge nanowires tracked the density of In nanoparticles. High densities of Ge nanowires were obtained only with n-Si substrates decorated with a high density of In nanoparticles. Larger nanowires were also more readily observed with less dense In nanoparticles. Second, the diameters of the electrodeposited Ge nanowires

dx.doi.org/10.1021/nl301912f | Nano Lett. XXXX, XXX, XXX−XXX

tracked the diameters of the In nanoparticles, i.e., thicker Ge nanowires, were observed with larger In nanoparticles. Third, each Ge nanowire appeared to emanate from a single and distinct location on the electrode surface.

The correlations between In nanoparticle and Ge nanowire size/density are shown quantitatively in Figure 4. Figure 4a is a plot of the Ge nanowire density as a function of the In nanoparticle density, spanning a range of 19.3−207.5 objects μm^{-2}. The dashed line indicates the expected correlation if every In nanoparticle yields a single Ge nanowire. The cumulative data from four separate trials indicated that the correlation was closer to one Ge nanowire obtained for every two In nanoparticles, i.e., not every In nanoparticle facilitated the electrodeposition of a Ge nanowire under the employed conditions. In these experiments, In nanoparticle sizes were kept below 100 nm, and the majority of In nanoparticles were below 60 nm. Experiments performed with In nanoparticles larger than 100 nm showed the tendency to 'seed' the electrodeposition of multiple Ge nanowires (Figure S3, Supporting Information). Figure 4b illustrates that the electrodeposition protocol used to prepare the In nanoparticle films on n-Si yielded broad distributions with respect to nominal particle diameter. The asymmetries in the distributions partially reflect the insensitivity of the scanning electron microscopic analysis toward ultrasmall (<5 nm) In nanoparticles. Nevertheless, Figure 4c demonstrates that the observed size (width) distributions of the Ge nanowires closely followed the distributions in Figure 4b. Separately, Figure 4c also shows that the variation in diameter, as described by the distribution width, was slightly narrower for the electrodeposited Ge nanowires as compared to the parent In nanoparticles, particularly at higher densities.

Additional measurements were performed to elucidate the location of the In nanoparticle following electrodeposition of a Ge nanowire. Figure 5 presents a set of micrographs

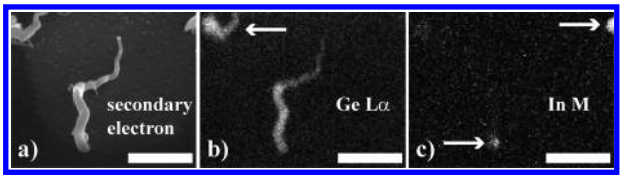

Figure 5. (a) Secondary electron scanning electron micrograph of an individual Ge nanowire electrodeposited at −2.0 V vs Ag/AgCl for 10 min. (b,c) Energy dispersive spectroscopic elemental mapping of same area in (a) with the detector channel for (b) the *Lα* line for Ge and (c) the *M* line for In. Images were collected with the sample tilted at 45°. Scale bars: 500 nm. Arrows highlight features of interest as discussed in the text.

highlighting the physical orientation of a single electrodeposited Ge nanowire and energy dispersive spectroscopic (EDS) maps of Ge and In, respectively. A matched secondary electron image of the nanowire in Figure 5a with a larger field of view is shown as Figure S4 (Supporting Information) and more clearly identifies a second nanowire located at the top left corner and a second In nanoparticle at the top right corner of Figure 5a (denoted with arrows in Figure 5b,c, respectively). EDS Ge mapping (Figure 5b) showed the nanowire was composed of Ge with no detectable In throughout the length. Similarly, In mapping (Figure 5c) showed localized concentrations of In only at the base of the Ge nanowire and not at the tip, as described in Figure 1a.

The presence of a metallic nanoparticle at the base of each Ge nanowire suggested that every Ge nanowire was electrically addressed and accordingly electrochemically active. To test this hypothesis, the activity of as-prepared Ge nanowire film electrodes as Li^+ battery anodes was explored. For Li^+ battery applications, Ge is an attractive anode material since it has a larger theoretical charge−discharge capacity than graphite (1624 mA h g^{-1} for $Li_{4.4}Ge$ vs 372 mA h g^{-1} for LiC_6) and supports faster Li^+ diffusivity than Si, facilitating Li^+ batteries with faster charge−discharge times.[20−25] A critical disadvantage with Ge as an electrode in Li^+ batteries is the large volumetric expansion upon Li^+ insertion which effectively pulverizes the material and limits the total lifetime of the electrode. In this capacity, the as-prepared Ge nanowires prepared here should show both high and long-lasting Li^+ charge−discharge capacities specifically due to their nanostructured, high aspect ratio electrode form factor. Since Si can also alloy with Li, a copper (Cu) foil was used as the electrode support for Ge nanowire electrodeposition for films that were interrogated as potential Li^+ battery electrodes. The inset to Figure 6a shows the appearance of a ca. 0.5 cm^2 Cu support before and after the Ge ec-LLS preparation step on Cu, highlighting the dark color of an as-prepared, dense Ge nanowire film. These Ge nanowire film electrodes were dried, massed, and then immediately tested as Li^+ battery electrodes without any further processing and/or application of binding agents or conductive carbon additives. The capacity and stability for Li^+ insertion−deinsertion of as-prepared Ge nanowires films were assessed in a two-electrode configuration with 1 M $LiPF_6$ in 2:1 (v/v) ethylene carbonate/diethyl carbonate.

Figure 6a shows the as-recorded first, second, third, and 26th charge−discharge curves for an electrodeposited Ge nanowire film electrode recorded at 1 C rate (1624 mA g^{-1}). The general profile of these chronopotentiograms mirrors previous reports of crystalline Ge charge−discharge curves at this C rate.[20−24,26] Similarly, the notable drop off in charging capacity after the first cycle is in accord with the known irreversible film formation at the solid−electrolyte interface of Ge Li^+ battery electrodes.[20,21] Control experiments performed with just the Cu foil and the Cu foil coated with In nanoparticles showed markedly different electrochemical behavior and much lower capacities for storing Li^+ (Figure S5, Supporting Information). The magnitude of the measured discharge capacity supports the notion that all of the Ge nanowires are electrochemically active. Figure 6b summarizes the as-recorded cycling data for an entire 26 cycle sequence. Following the second charge−discharge cycle, every subsequent cycle occurred with greater than 91% Coulombic efficiency. The discharge capacity slowly decreased over the course of the entire cycling period, dropping by less than 25% from the first to the twentieth discharge and consistent for Group IV Li^+ battery electrodes that alloy with Li and undergo volumetric expansion. The decay shown here is much less pronounced than for a planar crystalline Ge film (no effective Li^+ capacity after only seven cycles),[20] indicating the form factor of the as-electrodeposited Ge nanowires natively imparts stability against pulverization.

To gauge the overall performance quality of the Ge nanowire film electrodes prepared via ec-LLS, Table 1 summarizes the reported Li^+ capacity benchmarks for Ge and Ge-composite materials as Li^+ battery anodes at 1 C. The corrected charge and discharge capacities for the electrodeposited Ge nanowire film electrodes shown here have been corrected slightly for mass and Li^+ capacity contributions from the residual In

dx.doi.org/10.1021/nl301912f | *Nano Lett.* XXXX, XXX, XXX−XXX

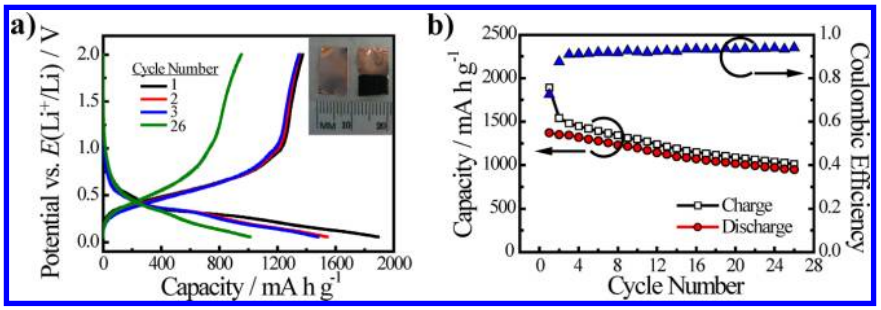

Figure 6. (a) First, second, third, and twenty-sixth charge−discharge curves for a Li^+ anode recorded at 1 C rate using an as-prepared Ge nanowire film electrodeposited onto a Cu support from 0.01 M $Na_2B_4O_7$ (aq) and 0.05 M GeO_2 (aq). Inset: optical photograph showing a Cu electrode support before and after Ge nanowire film electrodeposition. (b) Galvanostatic Li^+ (open squares) charge and (red circles) discharge cycling at 1 C rate using an as-prepared Ge nanowire film electrodeposited onto a Cu support from 0.01 M $Na_2B_4O_7$ (aq) and 0.05 M GeO_2 (aq). The Coulombic efficiencies for each charge−discharge cycle are indicated on the right *y*-axis (blue triangles).

Table 1. Reported Discharge Capacities for Ge Li^+ Insertion Anodes[a]

morphology	capacity, mA h g^{-1}	notes	ref
bulk	≪ 100	obtained at C/4 after 7 cycles	19
thin film	600	evaporated under vacuum	19
nanostructured thin film	1000	obtained at C/0.9, ion beam modified for nanostructuring	24
nanoparticles[b]	1460	prepared from $GeCl_4$ in dimethoxyethane, dried at 200 °C, butyl-capped	20
nanotubes[b]	765	prepared at 700 °C with Sb, coated with amorphous carbon	25
nanoporous film[b]	1415	prepared from $GeCl_4$, annealed at 800 °C, coated with amorphous carbon	23
nanowires	597	prepared from GeH_4 via VLS at 520 °C, annealed at 320 °C	21
nanowires	970	electrodeposited from GeO_2(aq) at room temp, no annealing	this work

[a]Reported at 1 C after 20 cycles unless noted otherwise. [b]Composite materials with Ge.

nanoparticles (Supporting Information). As evident from Table 1, the discharge capacity at 1 C for the Ge nanowires prepared here via ec-LLS compares favorably relative to conventional graphitic anodes (970 vs 330 mA h g^{-1}).[27] Compared specifically to the reported capacity of Ge nanowire film electrodes prepared via VLS,[22] the Ge nanowire films made with ec-LLS show a 160% larger discharge capacity and are among the most active pure Ge anode materials. We posit the mixed orientation of the crystallites along the Ge nanowire long axis as the likely source for the high capacities exhibited by the as-prepared Ge nanowire film electrodes, allowing for more facile Li^+ insertion as compared to undisrupted single-crystalline nanowires.

Only two reports have shown Ge nanomaterials with substantially larger discharge capacities after 20 cycles, achieved by adding a separate carbon coating for stability.[21,24] A comparison of those data[21,24] and the responses shown here indicate that the discharge capacities at the initial cycles are nominally equivalent. Although no additional measures were taken to stabilize and/or augment the native Li^+ capacities measured here, separate coating strategies[21,24] could in principle be applied to these Ge nanowires to impart added stability. Further, the Ge nanowire film electrodes investigated here were not rigorously optimized in terms of nanowire diameter, density, or length. Further refinements in these parameters ought to lead to improved performance characteristics. A final point to consider about the activity of these Ge nanowire film electrodes is the reproducibility of this method of preparation. Table S1 (Supporting Information) summarizes cycling data recorded at a faster charge−discharge rate (5 C) for several separately electrodeposited Ge nanowire film electrodes. With the unrefined conditions used here, capacity values varied by less than 12% between different electrodeposited Ge nanowire film electrodes.

These cumulative results highlight several advantages that ec-LLS has over both VLS and SLS strategies as well as alternative physical template-based electrochemical nanowire syntheses[28,29] for directly producing functional Ge nanowire electrodes under mild conditions. Both VLS and SLS routes for Ge nanowire growth require high (>300 °C) temperatures.[30,31] Physical template-based electrochemical strategies similarly require a high-temperature annealing step to effect an amorphous to crystalline transition.[28,29] The data here illustrate that nanowires are crystalline when prepared through the ec-LLS route and require no subsequent annealing. Both VLS and SLS methods as well as physical-template-based electrochemical methods require high-energy density, partially reduced chemical precursors, such as GeH_4,[32] GeI_2,[31] or diphenylgermane.[33] As embodied here, the ec-LLS process for Ge nanowires used a fully oxidized precursor (GeO_2) as the feedstock dissolved in aqueous electrolyte that was neither caustic nor highly acidic. VLS, SLS, and traditional electrochemical synthetic strategies do not tolerate the presence of water.[16,28,29]

The ec-LLS process yielded crystalline Ge nanowire films directly and controllably on multiple conductive substrates with control over nanowire diameters and densities without physical or chemical templates. In contrast, template-based electrochemical methods that require a hard, physical mold to define particular nanostructured morphologies necessitate an additional processing step(s) to remove the template. Separately, VLS methods require substrates that can withstand high process temperatures, greatly limiting the possible choices for electrode support materials. Although SLS is commonly performed with separate synthetic and processing steps for attaching nanowires to a current collector,[34] two variants of SLS processes also yield nanowires on substrates but without several of the advantages inherent to ec-LLS. Specifically, in contrast to both electrically controlled SLS (nonuniform nanowire deposition occurs between two closely spaced electrodes that support large, $\geq 10^5$ V m^{-1}, electric fields at high temper-

dx.doi.org/10.1021/nl301912f | Nano Lett. XXXX, XXX, XXX−XXX

atures)[35,36] and to substrate-nucleated SLS (metal catalysts are attached to an inert solid support),[37,38] ec-LLS incorporates precise electrochemical control to govern nanowire synthesis. As shown here, the current−time response during ec-LLS can be usefully monitored and fit to growth models to elucidate features of the nanowire deposition process. Conversely, the current response in electrically controlled SLS has an undetermined dependence on time and cannot be used to gain rapid and direct insight. The applied potential control with the 'flux' nanoparticle electrodes here in ec-LLS represents an additional handle not possible in substrate-nucleated SLS where only temperature and reactant concentration can be used to control nanowire growth.[37,38]

All of the factors involved in ec-LLS must be further studied to enable a wider breadth of potential applications. A quantitative description of how the interplay between the relative rates of mass transport in solution, electroreduction, dissolution, crystal nucleation, and precipitation impact the crystallinity, morphology, and conductivity of the electrodeposited semiconductor material is needed to prepare materials with higher crystallinity and precisely tunable morphological and electronic properties. Work dedicated to this point is ongoing in our lab and will be reported separately.

CONCLUSION

The cumulative data show that the ec-LLS process for crystalline Ge can occur at small, discrete In nanoparticles supported on either n-type silicon (Si) or copper (Cu) electrode substrates. The presented results indicate that the size and density of the crystalline Ge nanowires are readily tunable through control of the parent In nanoparticles and that each electrodeposited Ge nanowire is in direct electrical contact with the underlying electrode support through the In nanoparticle at the base of each nanowire. The activity of the as-prepared Ge nanowire film electrodes was competitive with existing, alternative protocols for producing nanostructured Ge battery anodes, with the important caveats that the method developed here was simpler, less energy intensive, and was performed entirely under benchtop conditions. Overall, the salient feature of this work is the demonstration of ec-LLS as a method to prepare directly a functional, high-activity nanomaterials-based device component. The data set shown here is a step toward the realization of simple processes that make fully functional energy conversion technologies entirely through benchtop chemistry and electrochemistry.

ASSOCIATED CONTENT

Supporting Information

A detailed description of the chemicals, materials, and methods used, a description of the protocols for In and Ge electrodeposition, the raw chronoamperometric data from Figure 1c, additional transmission electron microscopic data, scanning electron micrographs of Ge nanowire electrodeposition at large In nanoparticles, an alternate version of Figure 5a with a larger field of view, electrochemical responses for Li^+ charge−discharge at bare Cu and Cu electrodes coated with In nanoparticles, and electrochemical responses for Li^+ charge−discharge at Ge nanowire film electrodes at 5 C. This material is available free of charge via the Internet at http://pubs.acs.org.

AUTHOR INFORMATION

Corresponding Author

*E-mail: smald@umich.edu

Notes

The authors declare no competing financial interest.

ACKNOWLEDGMENTS

The authors thank the American Chemical Society Petroleum Research Fund (51339-DNI5) in support of this work. J.G. and X.H. recognize the University of Michigan Chemistry Department for Research Excellence Award fellowships. The FEI Nova Nanolab DualBeam FIB-SEM and JEOL 3011 TEM instruments used in this work are maintained by the University of Michigan Electron Microbeam Analysis Laboratory through NSF support (DMR-0320740 and DMR-0315633, respectively).

REFERENCES

(1) Hobbs, R. G.; Petkov, N.; Holmes, J. D. *Chem. Mater.* **2012**, *24* (11), 1975−1991.
(2) Williams, E. D.; Ayres, R. U.; Heller, M. *Environ. Sci. Technol.* **2002**, *36*, 5504−5510.
(3) Mirkin, C. A.; Tuominen, M. In *Nanotechnology Research Directions for Societal Needs in 2020*; Roco, M. C., Mirkin, C. A., Hersam, M. C., Eds.; Springer: Berlin, Germany, 2010.
(4) Carim, A. I.; Collins, S. M.; Foley, J. M.; Maldonado, S. *J. Am. Chem. Soc.* **2011**, *133*, 13292−13295.
(5) Wagner, R. S.; Ellis, W. C. *Appl. Phys. Lett.* **1964**, *4*, 89−90.
(6) Trentler, T. J.; Hickman, K. M.; Goel, S. C.; Viano, A. M.; Gibbons, P. C.; Buhro, W. E. *Science* **1995**, *270*, 1791−1794.
(7) Chen, X. Z.; Sportouch, S.; Sieve, B.; Brazis, P.; Kannewurf, C. R.; Cown, J. A.; Patschke, R.; Kanatzidis, M. G. *Chem. Mater.* **1998**, *10*, 3202−3211.
(8) Jolibois, P. *C. R. Chim.* **1910**, *150*, 106−108.
(9) Usui, S.; Yamasaki, T.; Shimoizaka, J. *J. Phys. Chem.* **1967**, *71*, 3195−3202.
(10) Dawson, B. D.; Lee, S. M.; Krim, J. *Phys. Rev. Lett.* **2009**, *103*, 205502(1-4).
(11) Han, Z. H.; Yang, B.; Qi, Y.; Cumings, J. *Ultrasonics* **2010**, *51*, 485−488.
(12) Zhang, M.; Efremov, M. Y.; Schiettekatte, F.; Olson, E. A.; Kwan, A. T.; Lai, S. L.; Wisleder, T.; Greene, H. E.; Allen, L. H. *Phys. Rev. B* **2000**, *62*, 10548−10557.
(13) Bottomley, D. J.; Iwami, M.; Uehara, Y.; Ushioda, S. *J. Vac. Sci. Technol. B* **1999**, *17*, 12−21.
(14) Bottomley, D. J. *Appl. Phys. Lett.* **1998**, *72*, 783−785.
(15) Huang, Q.; Bedell, S. W.; Saenger, K. L.; Copel, M.; Deligianni, H.; Romankiw, L. T. *Electrochem. Solid-State Lett.* **2007**, *10*, D124−D126.
(16) Fulop, G. F.; Taylor, R. M. *Annu. Rev. Mater. Sci.* **1985**, *15*, 197−210.
(17) Butler, J. N.; Dienst, M. *J. Electrochem. Soc.* **1965**, *112*, 226−232.
(18) Hyde, M. E.; Compton, R. G. *J. Electroanal. Chem.* **2003**, *549*, 1−12.
(19) Penner, R. M. *J. Phys. Chem. B* **2002**, *106*, 3339−3353.
(20) Graetz, J.; Ahn, C. C.; Yazami, R.; Fultz, B. *J. Electrochem. Soc.* **2004**, *151*, A698−A702.
(21) Lee, H.; Kim, M. G.; Choi, C. H.; Sun, Y. K.; Yoon, C. S.; Cho, J. *J. Phys. Chem. B* **2005**, *109*, 20719−20723.
(22) Chan, C. K.; Zhang, X. F.; Cui, Y. *Nano Lett.* **2008**, *8*, 307−309.
(23) Laforge, B.; Levan-Jodin, L.; Salot, R.; Billard, A. *J. Electrochem. Soc.* **2008**, *155*, A181−A188.
(24) Park, M. H.; Kim, K.; Kim, J.; Cho, J. *Adv. Mater.* **2010**, *22*, 415−418.
(25) Rudawski, N. G.; Darby, B. L.; Yates, B. R.; Jones, K. S.; Elliman, R. G.; Volinsky, A. A. *Appl. Phys. Lett.* **2012**, *100*, 083111(1-4).
(26) Park, M. H.; Cho, Y. H.; Kim, K.; Kim, J.; Liu, M.; Cho, J. *Angew. Chem.* **2011**, *123*, 9821−9824.
(27) Zheng, H.; Zhang, L.; Liu, G.; Song, X.; Battaglia, V. S. *J. Power Sources* **2012**, *217*, 530−537.

(28) Al-Salman, R.; Mallet, J.; Molinari, M.; Fricoteaux, P.; Martineau, F.; Troyon, M.; El-Abedin, S. Z.; Endres, F. *Phys. Chem. Chem. Phys.* **2008**, *10*, 6233−6237.
(29) Al-Salman, R.; Endres, F. *J. Mater. Chem.* **2009**, *19*, 7228−7231.
(30) Wu, Y. Y.; Yang, P. *J. Am. Chem. Soc.* **2001**, *123*, 3165−3166.
(31) Lu, X.; Fanfair, D. D.; Johnston, K. P.; Korgel, B. A. *J. Am. Chem. Soc.* **2005**, *127*, 15718−15719.
(32) Adhikari, H.; McIntyre, P. C.; Marshall, A. F.; Chidsey, C. E. D. *J. Appl. Phys.* **2007**, *102*, 094311(094315).
(33) Hanrath, T.; Korgel, B. A. *Adv. Mater.* **2003**, *15*, 437−440.
(34) Chan, C. K.; Patel, R. N.; O'Connell, M. J.; Korgel, B. A.; Cui, Y. *ACS Nano* **2010**, *4*, 1443−1450.
(35) Dorn, A.; Allen, P. M.; Bawendi, M. G. *ACS Nano* **2009**, *3*, 3260−3265.
(36) Dorn, A.; Wong, C. R.; Bawendi, M. G. *Adv. Mater.* **2009**, *21*, 3479−3482.
(37) Wang, F.; Wayman, V. L.; Loomis, R. A.; Buhro, W. E. *ACS Nano* **2011**, *5*, 5188−5194.
(38) Ouyang, L.; Maher, K. N.; Yu, C. L.; McCarty, J.; Park, H. *J. Am. Chem. Soc.* **2007**, *129*, 133−138.